Phase Diagram and Electrical Conductivity of High Energy-Density Water from Density Functional Theory

Thomas R. Mattsson and Michael P. Desjarlais

HEDP Theory and ICF Target Design, MS 1186, Sandia National Laboratories, Albuquerque, New Mexico 87185-1186, USA

(Received 4 January 2006; published 7 July 2006)

The electrical conductivity and structure of water between 2000–70 000 K and 0.1–3.7 g/cm^3 is studied by finite temperature density functional theory (DFT). Proton conduction is investigated quantitatively by analyzing diffusion, the pair-correlation function, and Wannier center locations, while the electronic conduction is calculated in the Kubo-Greenwood formalism. The conductivity formulation is valid across three phase transitions (molecular liquid, ionic liquid, superionic, electronic liquid). Above 100 GPa the superionic phase directly borders an electronically conducting fluid, not an insulating ionic fluid, as previously concluded. For simulations of high energy-density systems to be quantitative, we conclude that finite temperature DFT should be employed.

DOI: 10.1103/PhysRevLett.97.017801 PACS numbers: 61.20.Ja, 31.15.Ar, 51.50.+v, 62.50.+p

Knowledge of the electronic properties of water is essential for correctly describing the physics of, e.g., giant planets and shock waves in water. The behavior of water is complex due to the dual nature of conduction (ionic and electronic) and an intricate phase diagram. A predicted high-energy-density phase of water [1] was recently confirmed [2,3], adding superionic to the already rich variety of water phases: solid ice (h) to ice XI, liquid, and vapor. Here, we present calculations from first principles of both the ionic and electronic conductivity of water for a wide range of phase space in temperature and pressure, providing quantitative knowledge where little or no previous data are available. The calculations employ a finite temperature Fermi occupation of the electronic states [4], leading to a change in the predicted phase diagram.

Although a qualitative picture of water electrical conductivity has emerged, founded on experiments [5–7] and simulations [1–3,8], much needed quantitative information is scarce. Since experiments can only access certain areas of the phase diagram, and require modeling as a part of the analysis, calculations from first principles arise as a main approach. Density functional theory (DFT) calculations were done with VASP [9], where the Kohn-Sham equations [10] are solved in a plane-wave basis set. Projector augmented wave potentials [11] are used with PBE [12] for exchange or correlation. A Wannier center projection is made for each time step [13]. Most simulations were done using the deuterium mass, reducing computational cost. Both H_2O and D_2O were, however, examined for 2000 K at 2.3 and 3 g/cm^3, yielding a diffusion isotope effect of 1.3, close to the classical $\sqrt{2}$ [14]. A 900 eV plane-wave cutoff energy was chosen to give pressures converged to within 2%. The occupation of bands is set by a Fermi distribution [4]. Our calculations hence differ from the method used in previous studies [1–3,8], where the computationally efficient scheme by Car and Parrinello [15], propagating the electronic degrees of freedom close to the zero-temperature Born-Oppenheimer surface, was used [16,17]. The simulations are in the NVT ensemble using a Nosé thermostat. Pressures, energy, and other properties are calculated as averages after equilibration. The electronic conductivity is calculated using the Kubo-Greenwood formula [18] on 15–20 snapshots from the molecular-dynamics (MD) simulation. About 8 empty bands per water molecule are included in these calculations. Convergence of DFT simulations is of utmost importance [19]. Depending on density and temperature, simulation cells and times vary [20,21]. The gamma point is used for most MD simulations [22] while the mean value point (1/4, 1/4, 1/4) is used for conductivity calculations [21,22]. By a partition of the hydrogen diffusion and a robust method of defining bonds in dense systems, we calculate ionic conduction through the transition from insulating molecular liquid to fully dissociated ionic liquid. The equation of state, ionic conductivities, and electronic conductivities are thus calculated employing a common theoretical platform.

The calculated phase diagram is presented in Fig. 1. With increasing pressure, molecular water dissociates into an ionic liquid, followed by oxygen atoms freezing into the superionic phase. At higher temperature, the fluid is electronically conducting. We find that above 4000 K and 100 GPa, the fluid bordering the superionic phase is conducting. Earlier works instead have the superionic phase bordering an insulating fluid, with a transition to metallic fluid at 7000 K and 250 GPa [1]. This is not a revision without consequences, since the Neptune isentrope [1] is located in this region. The reason for our different result is the finite temperature treatment of the electronic degrees of freedom. By changing the temperature of the Fermi distribution, the electronic structure switches from a metal to an insulator. The effect is documented in Table I and illustrated in Fig. 2. At normal conditions, PBE underestimates the band gap for water

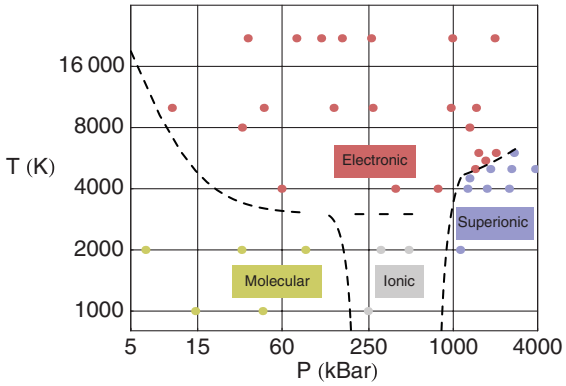

FIG. 1 (color). Theoretical phase diagram for water in the HEDP regime, each point represents a DFT-MD simulation. Molecular liquid—no dissociation of H_2O (yellow). Insulating ionic liquid—dissociation of H_2O and a gap in the electronic structure (gray). Superionic—very small O diffusion coefficient and gap in the electronic structure (blue). Electronically conducting ionic fluid—dissociation of H_2O, no gap in the electronic structure (red). The dashed lines are guides to the eye. The transition from superionic phase to the conducting fluid shows little hysteresis in the phase change, as can be inferred from the dense sampling in that region.

(4.4 vs 6.8 eV). The band closure observed in the simulations, however, is caused by a combination of density, pressure, molecular dissociation, and electronic temperature. It is hence impossible to estimate the true band gap by comparisons to normal conditions. Quantum Monte Carlo (QMC) simulations would provide valuable information, however, QMC is still computationally well beyond reach for this system. The importance of considering the thermal population of electronic states when performing DFT simulations in the high energy-density physics (HEDP) region is a general finding, independent of the outcome of future calculations, or experiments, for this particular system.

TABLE I. Electronic component of the dc conductivity (σ), average occupations (f_i) and energy (ϵ_i) difference $\Delta E = \epsilon_{\mathrm{LU}} - \epsilon_{\mathrm{HO}}$ of highest occupied (HO) and lowest unoccupied (LU) bands (defined when $T_e = 0$) when changing the electronic temperature. Two alternative techniques for smearing, Gaussian and Methfessel-Paxton, both yield gaps. The transition is seen for both 54 and 128 molecules cells. Units are molecules/cell, g/cm^3, Kelvin, $1/(\Omega\ \mathrm{m})$, occupation, and eV.

n	ρ	T_{ion}	T_e	$\log_{10}(\sigma)$	f_{HO}	f_{LU}	ΔE
54	2.5	4000	1000	0.7	1.98	0.03	1.53
54	2.5	4000	2000	1.2	1.97	0.04	1.74
54	2.5	4000	4000	3.84	1.63	1.25	0.38
128	2.5	4000	4000	3.78	1.63	1.36	0.26
128	2.5	4000	1000	1.0	1.96	0.05	1.01
54	3.0	6000	6000	4.5	1.43	1.25	0.22
54	2.7	8000	8000	5.0	1.28	1.18	0.14

The transition shown in Fig. 2 does not occur instantaneously with a different electronic temperature, it takes of the order 20–100 fs for the new electronic structure to develop, suggesting that reorientation of atoms is required. The transition is seen in the projected local orbital character of the highest occupied state; it changes character from S to P, as seen in Fig. 2. From a computational point of view, the transition time implies that postprocessing snapshots from zero K electronic temperature simulations is not equivalent to a full simulation using finite electronic temperature.

We propose that fast optical diagnostics could be used to investigate this transition, providing information on the electron-ion coupling in H_2O. Shock heating yields hot ions with cold electrons, a state we predict is an insulator. As the system equilibrates through ion/electron scattering, we anticipate a transition to electronic conduction.

Understanding the phase transition from a molecular fluid to a fully dissociated ionic fluid is important for modeling electrical breakdown and other phenomena in shocked water. In this region, a fraction of the hydrogen atoms are dissociated (conducting) while others remain bound as H_2O (nonconducting). Proton diffusion in normal state water occurs via a structural diffusion mechanism involving H^+, OH^-, and H_3O^+ [14,23].

We use Wannier centers (WC) [13,21] to characterize the charge transport. In water at 1000 K/1 g/cm^3, all H atoms are located 0.5 A from a WC; they are bound as H_2O. An *excess* proton, under the same conditions, moves on a path taking it at a distance of 0.75–1.15 A from two or three WCs, simultaneously, before reattaching as a H_3O^+. We find a striking similarity to this behavior in the WC dynamics of the denser systems: H atoms are either bound ($r_{\mathrm{WC-H}} \approx 0.5$) or they are mobile ($0.75 \leq r_{\mathrm{WC-H}} \leq 1.15$

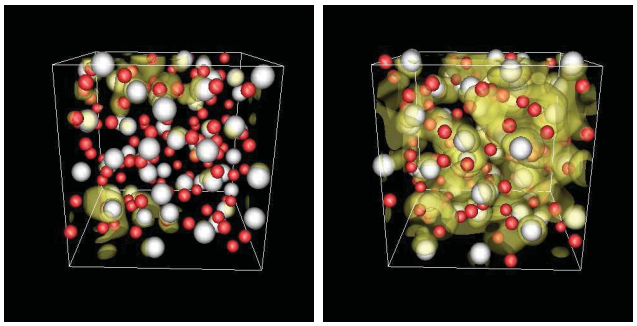

FIG. 2 (color). Snapshots of the structure (oxygen atoms are white, hydrogen atoms red) at $T = 4000$ K and $\rho = 2.5$ g/cm^3. Superimposed is a constant-electron-density surface (gold) projected from the HO state. Using the true temperature induces a shift from S to P character, changing the structure from being localized to spanning the cell, enabling conduction. The shift takes 20–100 fs to appear after changing the electronic temperature from $T_e = 1000$ K to $T_e = 4000$ K. The left snapshot is taken from this transition period, the right snapshot after the system is in equilibrium at $T_e = 4000$ K.

A). Since our findings are consistent with the established proton diffusion mechanism [14,23], we conclude that $+e$ charged protons dominate the conduction also under warm dense conditions.

Instead of analyzing these short-lived complexes, however, we focus on the *nonconducting* hydrogen motion—the transport of hydrogen taking place as H_2O diffusion. The fraction of H atoms bound as H_2O is γ, diffusing with the oxygen diffusion coefficient D_O. With D_H being the diffusion coefficients for *all* hydrogen atoms and D_{H^*} that for all hydrogen species except H_2O, the following relationship holds: $D_H = (1-\gamma)D_{H^*} + \gamma D_O$. Since D_O and D_H are independently calculated in the simulation [24] the conducting part of the mass transport is

$$D_{H^*} = \frac{1}{(1-\gamma)}\left(1 - \gamma\frac{D_O}{D_H}\right)D_H. \quad (1)$$

Although, by construction, D_{H^*} is insensitive to γ [25], we must define "bound". To distinguish scattering from bonds, we consider two atoms bound if they are within a cutoff distance during a time interval. We use the pair-correlation function, with $g(r) = 1$; beyond this point, the concept of bond weakens rapidly. Using the minimum of $g(r)$ has been proposed [3] but the minimum is often flat and leads to very large bonded complexes [26]. Results should not be sensitive to the specific choice of cutoff. Table II shows that it is meaningful to extract the H_2O fraction, γ, in the transition regime between molecular and ionic liquid. Although the ions H^+, OH^-, and H_3O^+ can be considered stable over several fs, the absolute fractions of them depend sensitively on both cutoff criteria, underscoring the difficulty to quantify composition in warm dense systems.

Figure 3 shows calculated conductivity (ionic and electronic) with available experimental data. At 2000 K there is only proton conduction. At 4000 K, the ionic and electronic contributions in the fluid are comparable, while the superionic phase, as expected [1], exhibits a surpressed electronic conductivity. At 6000 K, electronic conduction begins to dominate, and at 8000 K it is an order of magnitude larger than the contribution from protons. Above 22 000 K, water is dissociated and ionization is significant; the increase in density of states for larger specific volume maintains conductivity at low density. Figure 3 displays how Eq. (1) yields a rapid onset of conductivity with increased density due to pressure induced dissociation. Ignoring the nonconducting hydrogen motion results in overestimation of the conductivity. We predict that experiments at 1.5 g/cm^3 will show a very low conductivity. Finally, we note that in the fully dissociated regime there is no difference between the new formulation and the standard relationship between diffusion and conduction.

TABLE II. Distribution of species (mole per mole O) at 2000 K, 2 g/cm^3 when changing the bond cut-off distance, r_{cut}, and steady bond time, τ_{cut}. The fractions used in Eq. (1) are given in bold. The small deviations from neutrality are due to species not included in the table.

τ_{cut}	= **12.5** fs			
r_{cut} (A)	H	OH	H_3O	H_2O
1.10	0.20	0.20	0.012	0.78
1.16	**0.12**	**0.14**	**0.04**	**0.82**
1.20	0.06	0.10	0.06	0.83
1.30	0.006	0.047	0.15	0.81
r_{cut}	= **1.16** A			
τ_{cut} (fs)	H	OH	H_3O	H_2O
10	0.12	0.15	0.04	0.81
20	0.06	0.10	0.06	0.84
45	0.02	0.07	0.07	0.86

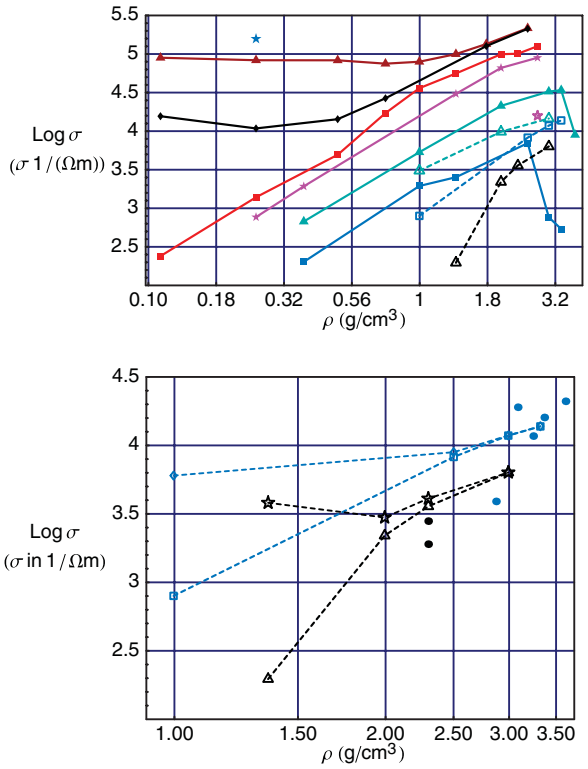

FIG. 3 (color). Upper: electronic conductivity (filled symbols and full lines) and ionic conductivity (open symbols and dashed lines) of water as a function of density for different temperatures: 70 (blue star), 44 (dark red triangles), 22 (black diamonds), 10 (red squares), 8 (magenta stars), 6 (turquiose triangles), 4 (blue squares), and 2 kK (black triangles). The sharp drops in conductivity for 4000 and 6000 K at 2.5 and 3.2 g/cm^3, respectively, corresponds to entering the superionic phase (see Fig. 1.) Lower: Ionic conductivity, as calculated for D_2O and scaled by 1.3 to compare to H_2O experiments. 2000 K from Eq. (1) (black triangles) and using the full hydrogen diffusion (black stars). 4000 K from Eq. (1) (blue squares) and using the full hydrogen diffusion (blue diamonds). Experimental data single shock at approximately 2000 K [5] (black circles) and multiple shock data between 2000 and 6000 K [6] (blue circles).

Recent optical measurements [7] demonstrate a gradual onset of reflectivity along the principal Hugoniot, followed by saturation at $R \approx 0.4$. We find the following reflectivities: 0.1 (4000 K, 2.5 g/cm^3), 0.2 (8000 K, 2.7 g/cm^3), 0.3 (10 000 K, 2.7 g/cm^3), 0.4 (22 000 K, 2.5 g/cm^3), and 0.3 (44 000 K, 1.8 g/cm^3), well in line with the experimental data [7]. Our calculations thus agree with experiments for total conductivity and reflectivity.

In summary, our comprehensive analysis of conduction in water reveals a rapid transition to ionic conduction at 2000 K and 2 g/cm^3, while electronic conduction dominates at temperatures at and above 6000 K. The phase diagram of water is further delineated in the HEDP region, with the superionic phase bordering a conducting fluid above 4000 K and 100 GPa. The resulting increase in electrical conductivity will affect calculations of thermophysical conditions in giant planets as well as how conduction is analyzed in shocked water (electrical breakdown). For first-principles simulations of HEDP systems to be of high fidelity, we show that it is important to include a thermal distribution of the electronic degrees of freedom. We anticipate this work will influence future DFT simulations in the HEDP regime.

We acknowledge fruitful discussions with Peter Schultz and Larry Warne. We thank Tom Mehlhorn for supporting our work and Martijn Marsman for the early opportunity to perform a Wannier center analysis in VASP. The LDRD office at SNL supported this work. Sandia is a multiprogram laboratory operated by Sandia Corporation, a Lockheed Martin Company, for the United States Department of Energy's National Nuclear Security Administration under Contract No. DE-AC04-94AL85000.

[1] C. Cavazzoni, G. L. Chiarotti, S. Scandolo, E. Tosatti, M. Bernasconi, and M. Parrinello, Science **283**, 44 (1999).
[2] A. F. Goncharov *et al.*, Phys. Rev. Lett. **94**, 125508 (2005).
[3] N. Goldman, L. E. Fried, I. Feng, W. Kuo, and C. J. Mundy, Phys. Rev. Lett. **94**, 217801 (2005).
[4] N. D. Mermin, Phys. Rev. **137**, A1441 (1965).
[5] A. C. Mitchell and W. J. Nellis, J. Chem. Phys. **76**, 6273 (1982).
[6] R. Chau *et al.*, J. Chem. Phys. **114**, 1361 (2001).
[7] P. M. Celliers, Phys. Plasmas **11**, L41 (2004).
[8] E. Schwegler, G. Galli, F. Gygi, R. Q. Hood, Phys. Rev. Lett. **87**, 265501 (2001).
[9] G. Kresse and J. Hafner, Phys. Rev. B **47**, R558 (1993); **49**, 14 251 (1994); G. Kresse and J. Furthmüller, Phys. Rev. B **54**, 11 169 (1996).
[10] P. Hohenberg and W. Kohn, Phys. Rev. **136**, B864 (1964); W. Kohn and L. J. Sham, Phys. Rev. **140**, A1133 (1965).
[11] P. E. Blöchl, Phys. Rev. B **50**, 17 953 (1994); G. Kresse and D. Joubert, Phys. Rev. B **59**, 1758 (1999).
[12] J. P. Perdew, K. Burke, and M. Ernzerhof, Phys. Rev. Lett. **77**, 3865 (1996).
[13] I. Souza, N. Marzari, and D. Vanderbilt, Phys. Rev. B. **65**, 035109 (2001); K. Leung and M. Marsman (to be published).
[14] Noam Agmon, Chem. Phys. Lett. **244**, 456 (1995).
[15] R. Car and M. Parrinello, Phys. Rev. Lett. **55**, 2471 (1985).
[16] The Car-Parrinello method has been extended to finite temperature [17], however, no water simulations have been performed, to our knowledge, in that framework.
[17] A. Alavi, J. Kohanoff, M. Parrinello, and D. Frenkel, Phys. Rev. Lett. **73**, 2599 (1994).
[18] M. P. Desjarlais, J. D. Kress, and L. A. Collins, Phys. Rev. E **66**, 025401(R) (2002).
[19] A. E. Mattsson *et al.*, Model. Simul. Mater. Sci. Eng. **13**, R1 (2005).
[20] All shown results for $\rho \geq 1$ g/cm^3 are for 54 molecules. Ten molecules were used for the lowest density $\rho = 0.11$ g/cm^3, 16, and 27 molecules for progressively denser points. Convergence tests were made up to 128 molecules. Simulation times are between 2 and 20 ps depending on the correlation time for each (T, ρ) point. A liquid cell at normal conditions was used as initial structure and the density was changed in steps, followed by equilibration.
[21] See EPAPS Document No. E-PRLTAO-97-036628 for additional information regarding convergence of the density functional theory calculations presented here. It also contains additional information on the Wannier center calculations reported in the Letter and additional references. For more information on EPAPS, see http://www.aip.org/pubservs/epaps.html.
[22] Representative convergence tests were made for both MD and conductivity calculations. The direct superionic/metallic fluid transition was confirmed using a $2 \times 2 \times 2$ k-points mesh for MD. At 4000 K/2.5 g/cm^3 the conductivity changes less than 10% when using 1, 4, 14, and 32 irreducible k points; a finding well in line with our past experience from conductivity calculations of large disordered systems.
[23] D. Marx, M. E. Tuckerman, and M. Parrinello, Nature (London) **397**, 601 (1999).
[24] Diffusion coefficients are calculated using velocity-velocity correlation functions averaged over 5–15 ps, depending on density and pressure. The proton conductivity is calculated using the classic Kubo response formulation using a proton charge of $+e$, as motivated by earlier work [1] and the presented Wannier center analysis.
[25] Proton conduction is primarily manifested in the difference between D_H and D_O. Once a difference exists, whether fewer protons move faster or more protons move slower has little effect on the conductivity.
[26] With $r_{cut} = 1.7$ A at 3 g/cm^3, where the average O-O distance is 2.3 A, H-O bonds are counted well past the nearest oxygen atom, resulting in "bonded" complexes like H_4O_2. We focus on finding the fraction of nonconducting H_2O, for which there is no motivation to include anomalously long O-H bonds.